

out significant error. Let $\mathbf{E}^I(\mathbf{r}, t)$ be the electric field of the incident beam. Upon reflection this field evolves to $\mathbf{E}^R(\mathbf{r}, t)$ which is to be found. From the linearity of the wave equation it follows that $\mathbf{E}^R(\mathbf{r}, t)$ can be determined by studying the action of the interface upon each plane wave field

$$\mathbf{A}^I(\mathbf{k}) = \mathbf{f}_\perp(\mathbf{k}) \exp(i\mathbf{k} \cdot \mathbf{r} - i\omega t) \quad (1)$$

that constitutes $\mathbf{E}^I(\mathbf{r}, t)$, with $\omega = |\mathbf{k}|c$. According to Refs. [22, 23], we assume the polarization dependent amplitude of $\mathbf{A}^I(\mathbf{k})$ equal to $\mathbf{f}_\perp(\mathbf{k}) = \hat{\mathbf{f}} - \hat{\mathbf{k}}(\hat{\mathbf{k}} \cdot \hat{\mathbf{f}}) = a_p(\mathbf{k}) \hat{\mathbf{x}}_{\mathbf{k}} + a_s(\mathbf{k}) \hat{\mathbf{y}}_{\mathbf{k}}$ with

$$a_p(\mathbf{k}) = f_p + Vf_s \cot \theta, \quad a_s(\mathbf{k}) = f_s - Vf_p \cot \theta, \quad (2)$$

up to first order in U, V , and $\theta = \arccos(\hat{\mathbf{z}}_i \cdot \hat{\mathbf{z}})$. Here $\hat{\mathbf{f}} = f_p \hat{\mathbf{x}}_i + f_s \hat{\mathbf{y}}_i$ is a unit complex vector that fixes the polarization of the incident beam, and $\hat{\mathbf{y}}_{\mathbf{v}} = \hat{\mathbf{z}} \times \mathbf{v} / |\hat{\mathbf{z}} \times \mathbf{v}|$, $\hat{\mathbf{x}}_{\mathbf{v}} = \hat{\mathbf{y}}_{\mathbf{v}} \times \mathbf{v}$ denote a pair of mutually orthogonal real unit vectors that together with the arbitrary vector $\hat{\mathbf{v}} = \mathbf{v} / |\mathbf{v}|$ form a right-handed Cartesian reference frame $K_{\mathbf{v}} = \{\hat{\mathbf{x}}_{\mathbf{v}}, \hat{\mathbf{y}}_{\mathbf{v}}, \hat{\mathbf{v}}\}$ attached to \mathbf{v} .

When the beam is reflected at the interface, each plane wave evolves as: $\mathbf{A}^I(\mathbf{k}) \rightarrow \mathbf{A}^R(\mathbf{k})$ where

$$\mathbf{A}^R(\mathbf{k}) = [r_p(\theta_{\mathbf{k}}) a_p \hat{\mathbf{x}}_{\tilde{\mathbf{k}}} + r_s(\theta_{\mathbf{k}}) a_s \hat{\mathbf{y}}_{\tilde{\mathbf{k}}}] \chi(\tilde{\mathbf{r}}, t), \quad (3)$$

and $\chi(\tilde{\mathbf{r}}, t) = \exp(i\tilde{\mathbf{k}} \cdot \mathbf{r} - i\omega t) = \exp(i\mathbf{k} \cdot \tilde{\mathbf{r}} - i\omega t)$. The notation $\tilde{\mathbf{v}}$ indicates the mirror image of the vector \mathbf{v} with respect to the interface: $\tilde{\mathbf{v}} = \mathbf{v} - 2\hat{\mathbf{z}}(\hat{\mathbf{z}} \cdot \mathbf{v})$, with $\tilde{\mathbf{v}} \cdot \mathbf{u} = \mathbf{v} \cdot \tilde{\mathbf{u}}$ [24]. Moreover, $r_p(\theta_{\mathbf{k}})$ and $r_s(\theta_{\mathbf{k}})$ are the Fresnel reflection coefficients at incidence angle $\theta_{\mathbf{k}} = \arccos(\hat{\mathbf{k}} \cdot \hat{\mathbf{z}})$ for p and s waves, respectively. By direct calculation it is not difficult to show that, up to first order in U, V ,

$$\hat{\mathbf{x}}_{\tilde{\mathbf{k}}} = \hat{\mathbf{x}}_r - V \cot \theta \hat{\mathbf{y}} + U \hat{\mathbf{z}}_r, \quad (4)$$

$$\hat{\mathbf{y}}_{\tilde{\mathbf{k}}} = V \cot \theta \hat{\mathbf{x}}_r + \hat{\mathbf{y}} - V \hat{\mathbf{z}}_r, \quad (5)$$

$$r_\lambda(\theta_{\mathbf{k}}) = r_\lambda + Ur'_\lambda, \quad (6)$$

where $\lambda \in \{p, s\}$, $r_\lambda = r_\lambda(\theta)$, and $r'_\lambda = \partial r_\lambda(\theta) / \partial \theta$. With the use of Eqs. (2,4-6) into Eq. (3) we obtain

$$\mathbf{A}^R(\mathbf{k}) = \hat{\mathbf{x}}_r A_p^R(\mathbf{k}) + \hat{\mathbf{y}}_s A_s^R(\mathbf{k}) + \hat{\mathbf{z}}_r A_L^R(\mathbf{k}), \quad (7)$$

where, up to first order in U, V ,

$$A_\lambda^R(\mathbf{k}) = f_\lambda r_\lambda (1 + iX_\lambda U - iY_\lambda V) \chi(\tilde{\mathbf{r}}, t), \quad (8)$$

$$A_L^R(\mathbf{k}) = (f_p r_p U - f_s r_s V) \chi(\tilde{\mathbf{r}}, t). \quad (9)$$

Here, we have defined

$$X_p = -i \frac{\partial \ln r_p}{\partial \theta}, \quad Y_p = i \frac{f_s}{f_p} \left(1 + \frac{r_s}{r_p} \right) \cot \theta, \quad (10)$$

with $X_s = X_p|_{p \leftrightarrow s}$ and $Y_s = -Y_p|_{p \leftrightarrow s}$. The limit of specular reflection is achieved by letting $r_p \rightarrow 1$ and $r_s \rightarrow -1$ where Eq. (10) reduces to $X_p = 0 = X_s$

and $Y_p = 0 = Y_s$. Notice that from Eqs. (8-9) it follows that for a paraxial beam the longitudinal electric field energy density $|A_L^R|^2$ scales as $\sim \alpha^2$ and it is therefore negligible with respect to the transverse electric field energy density $|A_p^R|^2 + |A_s^R|^2$ that scales as $\sim 1 + 2\alpha$. Thus, up to first order in α , we can neglect the longitudinal term $A_L^R(\mathbf{k})$ and write $\mathbf{A}^R(\mathbf{k}) \simeq \hat{\mathbf{x}}_r A_p^R + \hat{\mathbf{y}}_s A_s^R$. Moreover, for small shifts X_λ and Y_λ one can write $1 + iX_\lambda U - iY_\lambda V \simeq \exp(iX_\lambda U - iY_\lambda V)$, and in the Cartesian coordinate system attached to the reflected beam $\chi(\tilde{\mathbf{r}}, t) = \exp[i(-UX + VY + WZ)] \exp(-i\omega t)$, with $X = k_0 x_r$, $Y = k_0 y$, and $Z = k_0 z_r$, where z_r is the distance from the waist of the incident beam to the quadrant detector measured along the trajectory of the beam. Thus, Eq. (8) can be rewritten as:

$$A_\lambda^R(\mathbf{k}) \simeq f_\lambda r_\lambda \chi(-X + X_\lambda, Y - Y_\lambda, Z, t). \quad (11)$$

The passage from the single plane wave field $\mathbf{A}^R(\mathbf{k})$ to the total electric field $\mathbf{E}^R(\mathbf{r}, t)$ is realized by substituting the plane wave scalar amplitude $\chi(\mathbf{r}, t)$ into Eq. (11), with the electric field scalar amplitude $E(\mathbf{r}, t)$ describing the spatial distribution of the incident beam. In the present case, as we want to study the behavior under reflection of OAM beams, we choose $E(\mathbf{r}, t) = \psi_\ell(\mathbf{r}) \exp(-i\omega t)$, being $\psi_\ell(\mathbf{r})$ the Laguerre-Gauss paraxial field with OAM index $\ell \in \{0, \pm 1, \pm 2, \dots\}$ and radial index $p = 0$: $\psi_\ell(X, Y, Z) \propto \exp[-(X^2 + Y^2)/(2\Lambda + i2Z)] (X + is_\ell Y)^{|\ell|}$, with $s_\ell = \text{sign}(\ell)$ and $\Lambda = k_0(k_0 w_0^2/2)$ denoting the dimensionless Rayleigh range of the beam with waist w_0 [25]. Thus, the transverse electric field of a Laguerre-Gauss beam reflected by a plane interface can be written as:

$$E_\lambda^R(\mathbf{r}, t) \simeq f_\lambda r_\lambda \psi_\ell(-X + X_\lambda, Y - Y_\lambda, Z) \exp(-i\omega t). \quad (12)$$

In this expression the terms X_λ and Y_λ are responsible for the GH [8] and IF [19] shifts of the center of the beam, respectively. These displacements can be assessed by measuring the position of the center of the reflected beam with a quadrant detector centered at $x_r = 0, y = 0$ along the reference axis z_r attached to the reflected central wave vector $\tilde{\mathbf{k}}_0 = k_0 \hat{\mathbf{z}}_r$. A quadrant detector has four sensitive areas, denoted with a, b, c, d in the inset of Fig. 1, each delivering a photocurrent I_a, I_b, I_c, I_d respectively, when illuminated. The two currents $I_x = (I_a + I_b) - (I_c + I_d)$ and $I_y = (I_b + I_d) - (I_a + I_c)$ are thus proportional to the x - and the y -displacement of the beam intensity distribution relative to the center of the detector, respectively.

If $\ell = 0$, $\psi_0(-X + X_\lambda, Y - Y_\lambda)$ reduces to a shifted fundamental Gaussian beam, and in the hypothesis of small deviations $X_\lambda, Y_\lambda \ll 1$, a straightforward calculation furnishes

$$\frac{I_x}{I} = N_0 \left(\Delta_{\text{GH}} + \frac{Z}{\Lambda} \Theta_{\text{GH}} \right), \quad \frac{I_y}{I} = N_0 \left(\Delta_{\text{IF}} + \frac{Z}{\Lambda} \Theta_{\text{IF}} \right), \quad (13)$$

where $I = I_a + I_b + I_c + I_d$, and $N_0 = \sqrt{2/(\pi\sigma^2)}$ with $\sigma^2 = (\Lambda/2)\sqrt{1+Z^2/\Lambda^2}$. Here we have defined the two spatial (Δ) and the two angular (Θ) shifts

$$\Delta_{\text{GH}} = \sum_{\lambda=p,s} w_\lambda \text{Re}(X_\lambda), \quad \Delta_{\text{IF}} = \sum_{\lambda=p,s} w_\lambda \text{Re}(Y_\lambda), \quad (14)$$

and

$$\Theta_{\text{GH}} = \sum_{\lambda=p,s} w_\lambda \text{Im}(X_\lambda), \quad \Theta_{\text{IF}} = \sum_{\lambda=p,s} w_\lambda \text{Im}(Y_\lambda), \quad (15)$$

respectively, where the nonnegative coefficients w_λ are defined as the fraction of the electric field energy with polarization $\lambda = p, s$ in the reflected beam:

$$w_\lambda \equiv \frac{|r_\lambda f_\lambda|^2}{|r_p f_p|^2 + |r_s f_s|^2}. \quad (16)$$

If $\ell \neq 0$, Eq. (13) becomes

$$\frac{I_x}{I} = N_\ell \left(\Delta_{\text{GH}}^\ell + \frac{Z}{\Lambda} \Theta_{\text{GH}}^\ell \right), \quad \frac{I_y}{I} = N_\ell \left(\Delta_{\text{IF}}^\ell + \frac{Z}{\Lambda} \Theta_{\text{IF}}^\ell \right), \quad (17)$$

where $N_\ell = N_0 \Gamma(|\ell| + 1/2) / [\Gamma(|\ell| + 1) \sqrt{\pi}]$ ($\Gamma(x)$ denotes the Gamma function), and

$$\begin{bmatrix} \Delta_{\text{GH}}^\ell \\ \Theta_{\text{IF}}^\ell \\ \Delta_{\text{IF}}^\ell \\ \Theta_{\text{GH}}^\ell \end{bmatrix} = \begin{bmatrix} 1 & -2\ell & 0 & 0 \\ 0 & 1 + |2\ell| & 0 & 0 \\ 0 & 0 & 1 & 2\ell \\ 0 & 0 & 0 & 1 + |2\ell| \end{bmatrix} \begin{bmatrix} \Delta_{\text{GH}} \\ \Theta_{\text{IF}} \\ \Delta_{\text{IF}} \\ \Theta_{\text{GH}} \end{bmatrix}. \quad (18)$$

Equation (18) clearly displays the mixing between spatial and angular GH and IF shift, occurring only for $\ell \neq 0$, and it is in agreement with the results presented in Ref. [19], apart from the factor “2” in front of ℓ [26]. Notice that the polarization dependence of the four ℓ -dependent shifts on the left side of Eq. (18) resides in the four ℓ -independent shifts on the right side of the same equation. It turns out that the 4×4 mixing matrix itself is polarization-independent. It should be noticed that in TIR, contrary to partial reflection, both GH and IF angular shifts Θ_{GH} and Θ_{IF} are identically zero since the Fresnel coefficients are purely imaginary [27]. Thus, in this case it follows from Eq. (18) that mixing vanishes.

III. EXPERIMENTAL SET-UP

Our experimental set-up is shown in Fig. 2. A home built HeNe laser ($\lambda_0 = 633 \text{ nm}$) is forced to operate in a single higher-order Hermite-Gaussian (HG_{nm}) mode with $m = 0$ by insertion of a $40\text{-}\mu\text{m}$ diameter wire normal to the axis of the laser cavity [28]. The HG_{n0} beam is sent through an astigmatic mode converter consisting of two cylinder lenses, with their common axis oriented at 45° relative to the intra-cavity wire. This introduces a Gouy phase which converts the HG_{n0} beam in a $\text{LG}_{\ell p}$

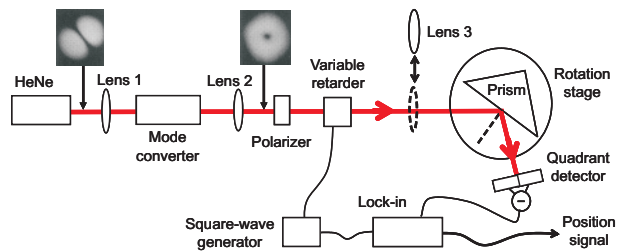


FIG. 2: (Color online) Experimental set-up. The insets show the HG_{10} and LG_{10} mode profiles. The quadrant detector measures the OAM controlled shift of the reflected beam in the plane of incidence (GH shift) and perpendicular to it (IF shift). Both the GH and the IF shift have a spatial and an angular contribution. See text for further details.

beam with $\ell = n$ and $p = 0$ [28]. Lenses 1 and 2 are used for mode matching; the beam leaving lens 2 is collimated with a waist parameter $w_0 = 775 \mu\text{m}$, a power of typically $600 \mu\text{W}$ and a polarization set by a linear polarizer. We have incorporated the option to greatly enhance the angular spread of the beam by inserting lens 3 ($f = 70 \text{ mm}$), leading to $w_0 = 19 \mu\text{m}$. Either with or without lens 3 present, the beam is externally reflected by the base plane of a glass prism (BK7, $n = 1.51$). We measured the polarization-differential shifts of the reflected $\text{LG}_{\ell 0}$ beam with a calibrated quadrant detector. We also obtained these shifts for the fundamental LG_{00} beam (= TEM_{00}) by simply removing the intra-cavity wire from the HeNe laser.

It follows from Eqs. (13-17) that using a collimated incident beam, i.e. $\Lambda \gg Z$, leads to total predominance of the spatial shift. On the other hand, the use of a focused beam, i.e. $\Lambda \ll Z$, leads to total predominance of the angular shift. These two extreme cases were realized in our experiment by removal respectively insertion of lens 3. Specifically, the value of the Rayleigh range $L = k_0 w_0^2 / 2$ was 2.96 m and 1.8 mm , respectively; as standard we have chosen the distance z_r between the beam waist and the quadrant detector to be 9.5 cm . We experimentally checked the angular nature of the shift (where expected) by verifying that the detector signal depended linearly on changes in z_r .

We performed all measurements by periodically (2.5 Hz) switching the polarization of the incident beam with a liquid-crystal variable retarder and by synchronously measuring (with a lock-in amplifier) the relative beam position for one polarization with respect to the other [5, 29]. Experimentally we were restricted to using the first-order LG modes ($\ell = \pm 1$) by the low gain of the HeNe laser.

IV. EXPERIMENTAL RESULTS AND COMPARISON WITH THEORY

Our experimental results for the polarization-differential shifts versus the angle of incidence are re-

ported in Fig. 3, together with the theoretical curves ($\ell = 0$ and $\ell = \pm 1$) which are based upon Eqs. (13-17). The four panels show the spatial and angular varieties of

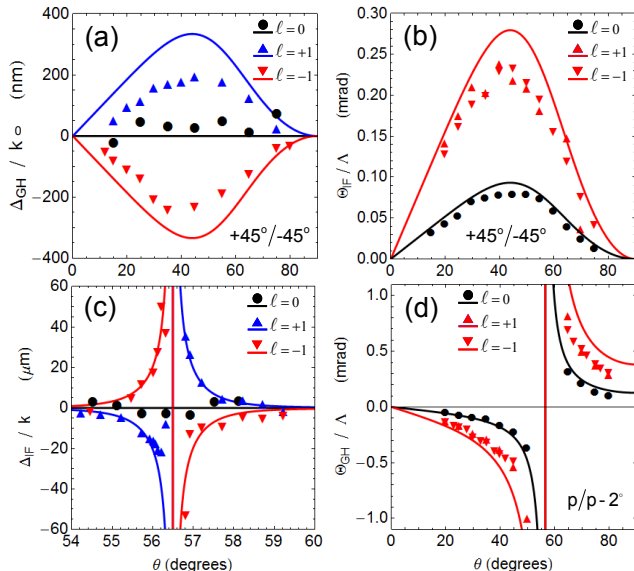


FIG. 3: (Color online) Reflective beam shift for partial dielectric reflection from an air-glass interface as a function of the angle of incidence. Plotted curves are the theoretical polarization-differential shifts for the two polarizations indicated in each panel. Experimental data and theoretical curves refer to $\ell = 0$ and $\ell = \pm 1$. The panels display the spatial GH shift (a), angular IF shift (b), spatial IF shift (c) and angular GH shift (d). Here $k_0 = 2\pi/\lambda_0$; see text for further details.

GH and IF shifts. Note that we have plotted here the true GH and IF shifts Δ/k_0 and Θ/Λ , respectively, and not the dimensionless shifts Δ and Θ . In each individual case the polarization modulation basis has been chosen such as to maximize the magnitude of the OAM effect. Fig. 4 shows a cartoon-like representation of the four cases that we address. The overall agreement between experiment and theory is reasonable if we realize that there is no fitting parameter involved; we ascribe the remaining discrepancies to insufficient modal purity of the LG_{10} beam (we are very sensitive to this since we use a quadrant detector).

Fig. 3a shows the spatial GH shift for a polarization basis of diagonal linear polarizations. In this case, the GH shift is absent for $\ell = 0$ but it appears for $\ell = \pm 1$; the sign of the shift reverses when going from $\ell = +1$ to $\ell = -1$. In Fig. 3b we show that the angular IF shift is different for $\ell = 0$ and $\ell = \pm 1$, using again diagonal linear polarizations. No difference occurs for $\ell = +1$ versus $\ell = -1$. Proceeding to Fig. 3c we observe an angular GH shift when using a linear polarization basis (s, p), for both $\ell = 0$ and $\ell = \pm 1$. Both cases show a dispersive resonance at the Brewster angle; for $\ell = 0$ these experimental results have been reported recently [5] whereas the data for $\ell = \pm 1$ (with opposite sign for $\ell = +1$ and $\ell = -1$) are

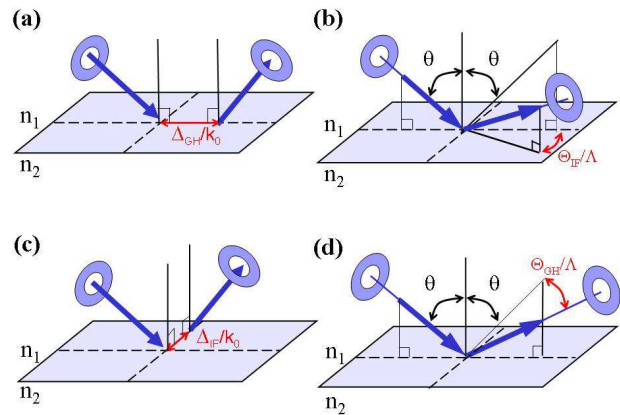


FIG. 4: (Color online) Reflection of an orbital-angular-momentum (OAM) carrying Laguerre-Gaussian (LG) beam at a dielectric interface. Depending on the input polarization this may lead to a longitudinal shift (Goos-Hänchen effect) or to a transverse shift (Imbert-Fedorov effect), where longitudinal and transverse refer to the plane of incidence. Each of these shifts consists of a spatial part and an angular part, which are observed, respectively, in the near field and in the far field of the LG beam. The magnitude of the shifts increases with the OAM index ℓ . Panel (a) shows the spatial Goos-Hänchen effect, panel (b) the angular Imbert-Fedorov effect, panel (c) the spatial Imbert-Fedorov effect and panel (d) the angular Goos-Hänchen effect. Note that Δ and Θ are dimensionless quantities; Λ and k_0 are the dimensionless Rayleigh range and the wavenumber of the LG beam, respectively. See text for further details.

new. Fig. 3d shows the OAM dependence of the spatial IF shift, observed in a linear polarization basis ($p, p-2^\circ$) [21, 30]. Here the shift is zero for $\ell = 0$ whereas it shows a dispersive Brewster resonance for $\ell = \pm 1$ (with opposite sign for $\ell = +1$ and $\ell = -1$).

Finally, we have confirmed experimentally that OAM did not affect spatial and angular GH and IF shifts in the TIR case (not shown); TIR was realized by flipping the glass prism in Fig. 2.

V. CONCLUSIONS

We have presented a unified theoretical description of how the Orbital Angular Momentum (OAM) of a light beam affects its kinematic degrees of freedom when the beam is reflected by a dielectric interface. Without OAM the reflection leads to four beam shifts relative to geometrical optics, namely the Goos-Hänchen (GH) and Imbert-Fedorov (IF) shifts, each of which may have a positional and an angular part. We introduce a 4×4 polarization-independent (but ℓ -dependent) coupling matrix that describes the OAM induced mixing of these four shifts when using a quadrant detector. Experimentally, we have confirmed this theory by measuring the four shifts as a function of the angle of incidence, for OAM values $\ell = 0$

and ± 1 . We have observed for the first time the OAM induced spatial GH shift as well as the OAM affected angular GH and IF shifts (see Fig. 3 a, b, c). Extension of all this from reflection to transmission (i.e. refraction) is straightforward.

Understanding these effects is important since they generally affect control of OAM beams by mirrors and lenses. The angular shifts are particularly interesting from a metrology point of view, both classically and quantum mechanically, since the corresponding transverse excursion of the beam center grows without limits when the beam propagates; this greatly promotes its detectability [5, 31].

VI. ACKNOWLEDGMENTS

We thank K.Y. Bliokh for stimulating us to measure the OAM-induced GH shift which acted as the seed of this paper. Our work is part of the program of the Foundation for Fundamental Research of Matter (FOM). It is also supported by the European Union within FET Open- FP7 ICT as part of the STREP program 255914 PHORBITECH. AA acknowledges support from the Alexander von Humboldt Foundation.

-
- [1] I. Newton, *Opticks*, reprinted by Dover Publications, Inc., New-York (1952); see Query 4 on p. 339.
- [2] F. Goos and H. Hänchen, *Ann. Phys.* **436**, 333 (1947).
- [3] C. Imbert, *Phys. Rev. D* **5**, 787 (1972).
- [4] F. I. Fedorov, *Dokl. Akad. Nauk SSSR* **105**, 465 (1955).
- [5] M. Merano, A. Aiello, M. P. van Exter, and J. P. Woerdman, *Nat. Photon.* **3**, 337 (2009).
- [6] O. Hosten and P. Kwiat, *Science* **319**, 787 (2008).
- [7] K. Y. Bliokh, A. Niv, V. Kleiner, and E. Hasman, *Nature Photonics* **2**, 748 (2008).
- [8] A. Aiello and J. P. Woerdman, *Opt. Lett.* **33**, 1437 (2008).
- [9] K. Artmann, *Ann. Phys. (Leipzig)* **2**, 87 (1948).
- [10] K. Y. Bliokh and Y. P. Bliokh, *Phys. Rev. Lett.* **96**, 073903 (2006).
- [11] K. Y. Bliokh and Y. P. Bliokh, *Phys. Rev. E* **75**, 066609 (2007).
- [12] D. Felbacq, A. Moreau, and R. Smaali, *Opt. Lett.* **28**, 1633 (2003).
- [13] Victor-O. de Haan, J. Plomp, T. M. Rekveldt, W. H. Kraan, A. A. van Well, R. M. Dalgliesh, and S. Langridge, *Phys. Rev. Lett.* **104**, 010401 (2010).
- [14] A. Mair, A. Vaziri, G. Weihs, and A. Zeilinger, *Nature* **412**, 313 (2001).
- [15] H. He, M. E. J. Friese, N. R. Heckenberg, and H. Rubinsztein-Dunlop, *Phys. Rev. Lett.* **75**, 826 (1995).
- [16] V. G. Fedoseyev, *Opt. Commun.* **193**, 9 (2001).
- [17] V. G. Fedoseyev, *J. Phys. A* **41**, 505202 (2008).
- [18] V. Fedoseyev, *Opt. Commun.* **282**, 1247 (2009).
- [19] K. Y. Bliokh, I. V. Shadrivov, and Y. S. Kivshar, *Opt. Lett.* **34**, 389 (2009).
- [20] H. Okuda and H. Sasada, *J. Opt. Soc. A* **25**, 881 (2008).
- [21] R. Dasgupta and P. K. Gupta, *Opt. Commun.* **257**, 91 (2006).
- [22] Y. Fainman and J. Shamir, *Appl. Opt.* **23**, 3188 (1984).
- [23] A. Aiello, C. Marquardt, and G. Leuchs, *Opt. Lett.* **34**, 3160 (2009).
- [24] R. F. Gragg, *Am. J. Phys.* **56**, 1092 (1988).
- [25] L. Mandel and E. Wolf, *Optical coherence and quantum optics* (Cambridge University Press, Cambridge, UK, 1995), 1st ed.
- [26] Here we quantify the GH and IF shifts via the photocurrents I_x/I and I_y/I delivered by the quadrant detector actually used in the experiment, respectively. This furnishes the *median* of the beam intensity distribution. Conversely, in Ref. [19] the same displacements are quantified via the *mean* of the intensity distribution. The difference between these two methods leads to both the trivial prefactor N_ℓ (experimentally eliminated by a detector calibration procedure), and the terms “ 2ℓ ” (instead of “ ℓ ”) in the mixing matrix (18).
- [27] A. Aiello, M. Merano, and J. P. Woerdman, *Phys. Rev. A* **80**, 061801(R) (2009).
- [28] M. W. Beijersbergen, L. Allen, H. E. L. O. van der Veen, and J. P. Woerdman, *Opt. Commun.* **96**, 123 (1993).
- [29] M. Merano, A. Aiello, G. W. 't Hooft, M. P. van Exter, E. R. Eliel, and J. P. Woerdman, *Opt. Expr.* **15**, 15928 (2007).
- [30] In this case maximum modulation of the beam shift is achieved by switching the (linear) polarization between p and s . However, instead of this we have chosen to switch the polarization between p and $p - 2^\circ$. This was done to reduce the very large intensity contrast occurring during $p \leftrightarrow s$ modulation and thus to minimize a parasitic cross-effect on the displacement as synchronously measured by the quadrant detector.
- [31] N. Treps, N. Grosse, W. P. Bowen, C. Fabre, H.-A. Bachor, and P. K. Lam, *Science* **301**, 940 (2003).